J Biomol NMR (2013) 57:37–45
DOI 10.1007/s10858-013-9763-5

ARTICLE

Dynamics of exocyclic groups in the *Escherichia coli* O91 O-antigen polysaccharide in solution studied by carbon-13 NMR relaxation

Maria Soltesova · Jozef Kowalewski · Göran Widmalm

Received: 19 February 2013 / Accepted: 17 July 2013 / Published online: 30 July 2013

Abstract Carbon-13 relaxation data are reported for exocyclic groups of hexopyranosyl sugar residues in the repeating unit within the *Escherichia coli* O91 O-antigen polysaccharide in a dilute D_2O solution. The measurements of T_1, T_2 and heteronuclear nuclear Overhauser enhancements were carried out at 310 K at two magnetic fields (16.4 T, 21.1 T). The data were analyzed using the standard and extended Lipari–Szabo models, as well as a conformational jump model. The extended version of the Lipari–Szabo and the two-site jump models were most successful for the hydroxymethyl groups of Gal and GlcNAc sugar residues. Different dynamics was found for the hydroxymethyl groups associated with different configurations (D-*gluco*, D-*galacto*) of the sugar residues, the latter being faster than the former.

Keywords Carbohydrates · Polysaccharide · Biopolymer · NMR spectroscopy · Model free approach · Two-site jump model

M. Soltesova · J. Kowalewski
Arrhenius Laboratory, Department of Materials and Environmental Chemistry, Stockholm University, 106 91 Stockholm, Sweden

M. Soltesova
Department of Low Temperature Physics, Faculty of Mathematics and Physics, Charles University in Prague, V Holesovickach 2, 180 00 Prague 8, Czech Republic

G. Widmalm (✉)
Arrhenius Laboratory, Department of Organic Chemistry, Stockholm University, 106 91 Stockholm, Sweden
e-mail: gw@organ.su.se

Abbreviations

DD	Dipole–dipole
CSA	Chemical shift anisotropy

Introduction

Polysaccharides are ubiquitous in Nature, for example cellulose in plants, amylose and amylopectin forming starch, carrageenans in seaweed as well as various types in living organisms such as heparan sulfate, chondroitin sulfate and other glycosaminoglycans in the animal kingdom (Rédini 2012). Capsular polysaccharides or loosely associated exopolysaccharides may be found around and associated to both Gram-positive and Gram-negative bacteria (Yother 2011). In the latter type, lipopolysaccharides (LPS) are an integral part of the outer membrane (Knirel and Volvano 2011). Besides the lipid A, which is anchored directly in the biomembrane, the LPS also has an additional region consisting of a dozen sugar residues, known as the core region; the O-antigen polysaccharide linked to the core is specific for each type of bacterial strain, although some of the bacteria may have the same polysaccharide structure due to the horizontal transfer of the genetic information (Lawrence 1999), and is typically built of 10–25 repeating units (RUs) having 2–7 sugar residues per RU (Stenutz et al. 2006). The structure and dynamics of polysaccharides are being studied by many different biophysical techniques (Carriere et al. 1993; Tang et al. 2004; Chytil et al. 2010; Jasnin et al. 2010) and NMR spectroscopy is an important one to this end (Hills et al. 1991; Hricovini et al. 1997; Vlachou et al. 2001; Henderson et al. 2003). Like for NMR investigations of proteins and nucleic acids the use of ^{13}C- and/or ^{15}N-isotope enrichment is a

powerful approach to obtain high quality data for polysaccharides in solution (Gitti et al. 1994; Kjellberg et al. 1999; Norris et al. 2012).

We have previously grown *Escherichia coli* O91 with either D-[UL-^{13}C]glucose, D-[1-^{13}C]glucose or D-[6-^{13}C]glucose and determined the primary structure (i.e., sugar components and their ring size, anomeric configurations, sequence and substituents) of its O-antigen polysaccharide, which has five sugar residues per RU (Fig. 1), and analyzed biosynthetic aspects of polysaccharide formation (Kjellberg et al. 1999). Subsequently, the polysaccharide from the D-[1-^{13}C]glucose growth was subject to a dynamics study (Lycknert and Widmalm 2004). This site-specifically labeled version of the polysaccharide has the ^{13}C-labels at, *inter alia*, the anomeric positions (C1) of the sugar residues thereby facilitating the investigation of the dynamics along the polymer chain. In the present study we have utilized the labeling that resulted from the D-[6-^{13}C]glucose growth, in which, *inter alia*, exocyclic groups of the sugar rings receive the isotopic labels (Fig. 1) and their dynamics can be studied while being part of the polysaccharide chain. The hypothesis is that the [6-^{13}C]-labeled sites should be sensitive to the dynamics of exocyclic CH_2OH groups and at the same time to the previously determined dynamics of the polymer chain from the [1-^{13}C]-labeled material. The superposition of the two types of dynamics would, on the Lipari–Szabo level of interpretation, lead to a description with additional local correlation times and/or lower or additional order parameters.

Materials and methods

The lipid-free polysaccharide grown on specifically labeled D-[6-^{13}C]glucose (Kjellberg et al. 1999) was used for NMR experiments at 310 K and a concentration employed previously for the relaxation studies, i.e., approximately 7 mM in D_2O solution with respect to labeled RUs (Lycknert and Widmalm 2004). The ^{13}C NMR assignments of the C6 atoms of hydroxymethyl groups were performed using the H2BC experiment (Nyberg et al. 2005) in conjunction with previously determined chemical shifts (Kjellberg et al. 1999) and were carried out on a Bruker AVANCE III 700 MHz spectrometer equipped with a 5 mm TCI Z-Gradient Cryoprobe. The ^{13}C NMR chemical shifts are reported in ppm relative to external 1,4-dioxane in D_2O (δ_C 67.40) as a reference.

Relaxation experiments were performed at a temperature of 310 K on Bruker Avance III 700 and Bruker Avance 900 spectrometers operating at magnetic fields of 16.4 T and 21.1 T, respectively. Both spectrometers were equipped with 5-mm TCI cryoprobes, with the probe on the 16.4 T instrument actually providing a somewhat better signal-to-noise ratio. For this reason, we typically used fewer scans at 16.4 T than at 21.1 T. The sample temperature was calibrated carefully using a deuterated methanol NMR chemical shift thermometer. Standard variable temperature control units of the spectrometers were used to regulate the temperature. The relaxation data collected are based on peak intensities (obtained after exponential weighting with a line broadening of 5 and 2 Hz at 16.4 and 21.1 T, respectively) of the resonances analyzed.

Carbon-13 longitudinal relaxation times (T_1) were measured using the standard ^{13}C-detected inversion-recovery method with broadband proton decoupling using the Waltz-16 scheme at the power level corresponding to a ^{1}H $\pi/2$ pulse duration of $\sim$80 μs ($B_1 \approx 3.1$ kHz); 12–16 variable delays between the inversion pulse and the read pulse were employed. The number of scans was 256 at the lower field and 1,024 at the higher field. The recycle delay was at least five times the longest T_1 and 4 dummy scans were used. The values of T_1 were obtained by three-parameter exponential fitting of the signal intensities using

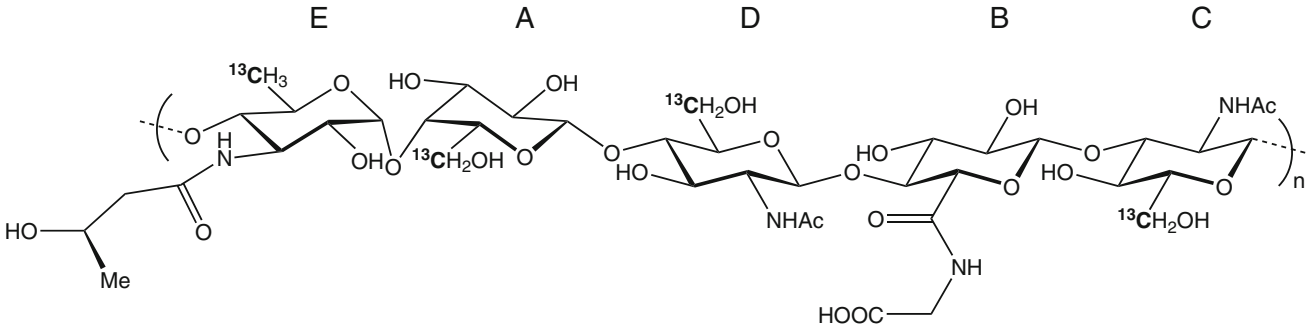

Fig. 1 Schematic of the *E. coli* O91 O-antigen polysaccharide, where the number of repeating units n $\approx$ 10. Sugar residues are denoted by **A–E** (Kjellberg et al. 1999; Lycknert and Widmalm 2004) and site-specific ^{13}C isotope labeled positions investigated herein are highlighted in *bold* characters

fitting routines provided by the instrument manufacturer. It is worthwhile to comment here on the possible deviations from the single exponential longitudinal relaxation for the CH_3 and CH_2 carbons, caused by cross-correlation effects. The methyl carbons can in general display double exponential relaxation (Werbelow and Grant 1977). As shown by Kay and Torchia (1991), the deviations from a single exponential behaviour become negligible under certain motional conditions. As discussed below, our system seems to fall in this range. The spin–lattice relaxation of the CH_2 groups is not a problem. As shown by Brondeau and Canet (Brondeau and Canet 1977), the proton decoupling suppresses the cross-correlations effects in such groupings, if the two protons are not magnetically equivalent.

Carbon-13 transverse relaxation times (T_2) were measured using the standard CPMG spin-echo experiment with ^{1}H 180° pulses to suppress the cross-correlation between the dipole–dipole (DD) and chemical shielding anisotropy (CSA) (Palmer et al. 1992; Kay et al. 1992). Constant echo time was used during the experiments, set to 500 μs at the lower field and to 250 μs at the higher field, while the number of echoes was varied in 12–16 loops. The number of scans was 512 at the lower field and 1,024 at the higher field. The recycle delay was set to the value at least five times higher than the longest T_1; 16 dummy scans were used. The values of T_2 were obtained by two-parameter exponential fitting of the signal intensities using fitting routines provided by the instrument manufacturer. The cross-correlation effects in transverse relaxation are likely to have more significant effects (Kay and Torchia 1991; Kay and Bull 1992; Zhu et al. 1995). While the DD–CSA cross-correlation effects are suppressed by the ^{1}H 180° pulses, the DD–DD effects are not. For the methyl carbons, Kay and Torchia (1991) recommended the use of initial decay rate to reduce the errors caused by dipolar cross-correlation effects. We follow this procedure and estimate the transverse relaxation rate from a few points at low numbers of CPMG cycles.

Nuclear Overhauser enhancement (NOE) was measured using the dynamic NOE experiment with the same decoupling power ($B_1 \approx 3.1$ kHz) during the NOE buildup time. Two experiments were recorded, one with a very long irradiation time ($> 5\ T_1$) and one with a very short irradiation time (1 ms). The NOE value was obtained as the ratio of the corresponding signal intensities in the two spectra. The recycle delay was always set very long, around ten times the longest T_1. The number of scans was 1,024 at the lower field and 2,048 at the higher field. Also the NOE measurements in CH_3 and CH_2 groups are affected by cross-correlations. As estimated by Kay and Torchia (1991), the errors should be rather limited in the range of relevance for this work. Another possible error source arises from the choice of saturation scheme applied during the NOE build-up period. As discussed by Ferrage et al. (2010), the Waltz-16 with the B_1 of about 3.1 kHz should not introduce uncertainties of more than a few percent.

The typical duration of the carbon-13 π/2-pulse was 12 μs at 16.4 T and 16 μs at 21.1 T. Spectral width was set to ∼150 ppm at 16.4 T and ∼65 ppm at 21.1 T. The accuracy of the T_1, T_2 and NOE measurements is estimated to be better than 3, 10 and 5 %, respectively. All experiments were carried out at least two times and average values are reported.

Least-squares fitting of the experimental relaxation data to the motional parameters was performed using in-house written MATLAB routines. The contributions of the relaxation parameters (T_1, T_2, NOE) to the given motional model were weighted according to their estimated errors $\sigma_{est,i}$ in per cent listed above. The target function was:

$$\chi^2 = \sum_{i=1}^{N} \left[\frac{\left(y_{i,expt} - y_{i,calc}\right)}{y_{i,expt}} \frac{1}{\sigma_{est,i}} \right]^2 \quad (1)$$

Reported values of relative errors of the fit were calculated as follows:

$$\text{Rel. err.} = \sqrt{1/(N-M) \sum_{i=1}^{N} \left[\left(y_{i,expt} - y_{i,calc}\right) / y_{i,expt} \right]^2} \quad (2)$$

where y_i denotes the calculated (*calc*) and experimental (*expt*) relaxation parameters, N is the number of experimental data and M is the number of fitted parameters for given model.

Theory

The most effective relaxation mechanism in the system under study is the dipole–dipole interactions between the carbon and the two directly bonded protons in the hydroxymethyl groups. Chemical shift anisotropy is usually negligible or has a minor contribution to the relaxation in such systems.

When the cross-correlation effects can be neglected, the longitudinal and transverse relaxation times (T_1 and T_2, respectively), as well as the NOE ($1 + \eta$) can be expressed in terms of spectral densities $J(\omega)$ taken at different linear combinations of carbon (ω_C) and proton (ω_H) Larmor frequencies as follows (Kowalewski and Mäler 2006):

$$T_{1,\mathrm{DD}}^{-1} = \frac{n_H}{4} d^2 [J_{CH}(\omega_H - \omega_C) + 3J_{CH}(\omega_C) + 6J_{CH}(\omega_H + \omega_C)] \quad (3)$$

$$T_{2,\mathrm{DD}}^{-1} = \frac{n_H}{8} d^2 [4J_{CH}(0) + J_{CH}(\omega_H - \omega_C) + 3J_{CH}(\omega_C) + 6J_{CH}(\omega_H) + 6J_{CH}(\omega_H + \omega_C)] \quad (4)$$

$$\begin{aligned}\mathrm{NOE} &= 1+\eta \\ &= 1+\frac{\gamma_H}{\gamma_C}\frac{6J_{CH}(\omega_H+\omega_C)-J_{CH}(\omega_H-\omega_C)}{J_{CH}(\omega_H-\omega_C)+3J_{CH}(\omega_C)+6J_{CH}(\omega_H+\omega_C)}\end{aligned} \tag{5}$$

The dipole–dipole coupling constant $d=-\frac{\mu_0}{4\pi}\gamma_H\gamma_C\hbar(r_{CH})^{-3}$ depends on the C–H distance, r_{CH}, as well as several universal constants (permittivity of vacuum μ_0, magnetogyric ratios for ^{13}C and ^{1}H, γ_C and γ_H respectively, and the reduced Planck constant $\hbar$), n_H denotes the number of hydrogens directly attached to the studied carbon; Eqs. (3)–(5) assume that the dynamics of different C–H vectors is equivalent.

The particular functional form of the spectral densities $J(\omega)$ depends on the motional model chosen to interpret the dynamics of the molecule. Under the assumption of the isotropic overall reorientation of the whole molecule (with the global correlation time τ_M) and, in addition, of a much faster restricted local motion, the Lipari–Szabo form of spectral densities can be employed (Lipari and Szabo 1982). The local motion is described by a local correlation time τ_e and a generalized order parameter S^2, and it is assumed to be statistically independent of the global motion.

$$J(\omega)=\frac{2}{5}\left[\frac{S^2\tau_M}{1+\omega^2\tau_M^2}+\frac{(1-S^2)\tau}{1+\omega^2\tau^2}\right] \tag{6a}$$

$$\tau^{-1}=\tau_M^{-1}+\tau_e^{-1} \tag{6b}$$

For interpretation of methyl dynamics (Skrynnikov et al. 2002; Millet et al. 2002; Chatfield et al. 1998), we can assume that the fast local motion consists predominantly of a fast methyl spinning and fast side-chain motions (torsional librations, bond angle fluctuations, fast rotameric transitions). All these processes are described by a single local correlation time τ_e, and a generalized order parameter S^2. Possible quantum effects in the methyl motion (Widmalm et al. 1991) are neglected. If we assume the ideal tetrahedral geometry for the methyl groups, the order parameter for the local motion can be written as $S^2=1/9S_{ax}^2$, where the factor 1/9 originates from fast methyl spinning and S_{ax}^2 reflects the rapid fluctuation of the methyl averaging axis. The Lipari–Szabo spectral density (LS-2 in the notation of Skrynnikov et al.) then attains the form:

$$J(\omega)=\frac{2}{5}\left[\frac{1}{9}S_{ax}^2\frac{\tau_M}{1+\omega^2\tau_M^2}+\left(1-\frac{1}{9}S_{ax}^2\right)\frac{\tau}{1+\omega^2\tau^2}\right] \tag{7a}$$

$$\tau^{-1}=\tau_M^{-1}+\tau_e^{-1} \tag{7b}$$

In more complicated cases it is necessary to account for a slower local motion, possibly outside of the extreme narrowing region, occurring besides the fast local motion. Clore et al. (1990) suggested an extension of the Lipari–Szabo model (also referred to as the extended Lipari–Szabo model), considering two kinds of uncorrelated local motions taking place on different timescales. These motions are characterized by two different correlation times τ_f and τ_s, and by two generalized order parameters S_f and S_s, for the faster and slower motions, respectively. The spectral density attains then the following form:

$$J(\omega)=\frac{2}{5}\left[\frac{S^2\tau_M}{1+\omega^2\tau_M^2}+\frac{\left(1-S_f^2\right)\tau_F}{1+\omega^2\tau_F^2}+\frac{\left(S_f^2-S^2\right)\tau_S}{1+\omega^2\tau_S^2}\right] \tag{8a}$$

$$\tau_F^{-1}=\tau_M^{-1}+\tau_f^{-1} \tag{8b}$$

$$\tau_S^{-1}=\tau_M^{-1}+\tau_s^{-1} \tag{8c}$$

If the faster motion can be assumed to be axially symmetric and independent of the slower motion, then the global generalized order parameter can be decomposed into $S^2=S_f^2S_s^2$.

For the case of a methyl group whose axis is subject to both fast and slow motional components, Skrynnikov et al. (2002) proposed also a more sophisticated model, denoted LS-4. This model is derived under different assumptions compared to that of Clore et al. (1990), but the two models become equivalent if $\tau_f \ll \tau_s, \tau_M$ and $\omega^2\tau_f^2 \ll 1$ (extreme narrowing for the fast motion).

The other dynamic model considered in this work describes specific motional processes in terms of random jumps (Ghalebani et al. 2008; London 1978). This model allows a simple description of local conformational changes, an important issue in interpretation of dynamics of polysaccharides. The conformational exchange can, in principle, be described as a two-site jump. Considering an internal motion and an overall isotropic reorientation, the spectral densities of a two-site jump model take the form:

$$J(\omega)=\frac{2}{5}\sum_m a_m J_m(\omega) \tag{9a}$$

$$\begin{aligned}J_m &= \frac{\left[1-4P(1-P)\sin^2(m\gamma_j)\right]\tau_M}{1+\omega^2\tau_M^2} \\ &\quad+\frac{4P(1-P)\sin^2(m\gamma_j)\tau'}{1+\omega^2\tau'^2}\end{aligned} \tag{9b}$$

$$\tau'^{-1}=\tau_M^{-1}+\tau_j^{-1} \tag{9c}$$

where τ_M denotes the global correlation time, τ_j stands for the jump correlation time (inverse jump rate), P is the population of one of the sites, γ_j is the jump *half*-angle (the jump occurs between $+\gamma_j$ and $-\gamma_j$) and the coefficients a_m with $m=0,1,2$ can be expressed as follows

$$a_0=\frac{1}{4}\left(3\cos^2\theta-1\right)^2 \tag{10a}$$

$$a_1=3\cos^2\theta\sin^2\theta \tag{10b}$$

$$a_2=\frac{3}{4}\sin^4\theta \tag{10c}$$

The angle θ is the angle between the C–H vector and the jump axis (C5–C6 bond in the case of hydroxymethyl groups in the polysaccharide under study).

As discussed by Kövér et al. (2004), the spectral densities of the random jump model can be re-written in the form analogous to the Lipari–Szabo formulation, with τ' of Eq. (9c) replacing τ in Eq. (6a) and the generalized order parameter given by the relation:

$$S^2 = \frac{1}{9} + \frac{8}{27}\left[1 - 4P(1-P)\sin^2\gamma\right] + \frac{16}{27}\left[1 - 4P(1-P)\sin^2 2\gamma\right] \quad (11)$$

For an ideal two-site jump ($P = 0.5$ and $\gamma = \pm 60°$) Eq. (11) yields $S^2 = 0.33$. The right-hand side of the Eq. (11) has a mathematical minimum for $P = 0.5$ and $\gamma \approx \pm 49°$ which leads to an order parameter $S^2 = 0.25$. This means that in principle it is not possible to interpret a generalized order parameter lower than 0.25 using this approach.

Equation (11) means that, in general, it is not possible to independently determine P and γ. If one of these parameters is known from an independent source, then the other one can be evaluated, thus allowing in principle a specific physical interpretation of the generalized order parameter.

Results and discussion

The O-antigen polysaccharide from *E. coli* O91 is built of repeating units consisting of five sugar residues labeled **A**–**E**, each of which is a hexopyranosyl entity containing six carbon atoms (Fig. 1). The amino sugars **C** and **D** are *N*-acetylated, residue **B** carries a glycinyl group and residue **E** has an (*R*)-3-hydroxybutyryl group as a substituent. The structural determination of the polysaccharide was carried out at 338 K and a magnetic field strength of 14.1 T (Kjellberg et al. 1999). At a lower temperature of 310 K and higher fields of 16.4 and 21.1 T used herein the ^{13}C NMR resonances of the three hydroxymethyl (CH_2OH) groups were resolved. The spectrum obtained at 16.4 T is shown in Fig. 2. The signals at 60.73, 60.87 and 61.95 ppm were assigned to the C6 atoms of residues **D**, **A** and **C**, respectively, by the application of the H2BC experiment (Nyberg et al. 2005). The C6 methyl group of residue **E** resonates at 17.05 ppm. In the previous ^{13}C NMR relaxation study based on the [1-^{13}C]-labeled material (Lycknert and Widmalm 2004) we were able to show that a minor C1 signal originated from the terminal sugar (**E**′) of the polysaccharide. In the presently investigated [6-^{13}C]-labeled polysaccharide minor resonances at 17.26 and 60.91 ppm, are consequently assigned to the residues **E**′ and **A**′ of the terminal RU, respectively, fully consistent with results from the earlier investigation and aspects of the polysaccharide biosynthesis (Stenutz et al. 2006). Already at the onset of the investigation of the dynamics of the hydroxymethyl groups by ^{13}C NMR spin-relaxation we note that the full-widths-at-half-maximum differ, $\nu^{C}_{1/2} \approx \nu^{D}_{1/2} > \nu^{A}_{1/2}$ (see Fig. 2).

For hexopyranosyl residues that have the D-*gluco*-configuration, i.e., in the $^4C_1$ conformation where the C4–O4 bond is equatorial, a conformational equilibrium between the *gauche-trans* (+65°) and the *gauche–gauche* (−65°) conformation of the ω torsion angle defined by O5–C5–C6–O6 is approximately 1:1 (Stenutz et al. 2002; Olsson et al. 2009; Zerbetto et al. 2009). For hexopyranosyl residues having the D-*galacto*-configuration, i.e., in the $^4C_1$ conformation where the C4–O4 bond is axial, a conformational equilibrium between the *gauche-trans* and the *trans-gauche* (180°) conformation of ω is approximately 2:1 (Stenutz et al. 2002) (Fig. 3). In the polysaccharide, the residues **C** and **D** are of the former type whereas residue **A** is of the latter.

The carbon-13 relaxation was measured for the resonances of hydroxymethyl group carbons in residues **A**, **C** and **D** and for the methyl group carbon in residue **E** at the magnetic fields of 16.4 T and 21.1 T. Although partial spectral overlap may occur for residue **A** with the **A**′ signal, the intensity of **A**′ is about ten times lower thus unlikely to affect the relaxation of **A** significantly. Experiments were carried out at the temperature of 310 K to ensure that the polysaccharide is mobile enough to avoid severe broadening of the resonances but its motion is still outside of the extreme narrowing limit. The results are reported in Table 1.

The small NOE factor (< 3) and field-dependent T_1 and T_2 relaxation times show that the motion of the polysaccharide is outside of the extreme narrowing limit. The frequency-dependent relaxation data can thus be

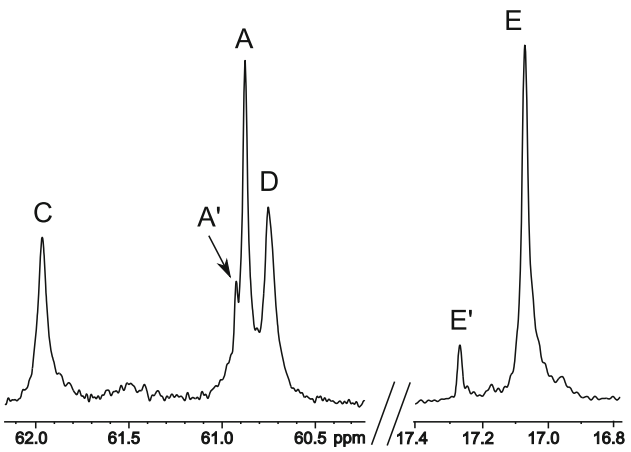

Fig. 2 Carbon-13 NMR spectrum of the site-specifically ^{13}C-labeled *E. coli* O91 O-antigen polysaccharide, obtained at 16.4 T and 310 K

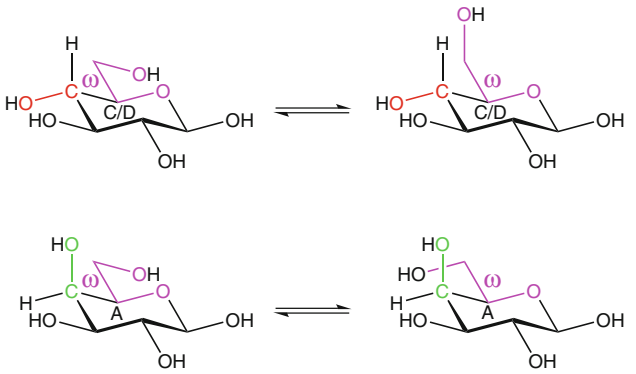

Fig. 3 Conformational equilibria of the ω torsion angle (magenta colored) for D-hexopyranose sugars in the $^4C_1$ conformation showing for the D-*gluco*-configuration (*red color* at C4) the *gauche-trans* conformation (*top*, *left*) and the *gauche–gauche* conformation (*top*, *right*) compared to the D-*galacto*-configuration (*green* color at C4) with the *gauche-trans* conformation (*bottom*, *left*) and the *trans-gauche* conformation (*bottom*, *right*). In the polysaccharide residues **C** and **D** have the D-*gluco*-configuration whereas residue **A** has the D-*galacto*-configuration, indicated by the *capital letters* in the pyranose rings

interpreted using Eqs. (3)–(5). It is evident that the relaxation data for the methyl group in residue **E** differ from the methylene group carbons data (residues **A**, **C** and **D**) quite significantly. Slight differences can be observed also between **A** on one hand and **C** and **D** on the other, which is consistent with the different configurations of the sugar rings of residue **A** compared to **C** and **D**.

The relaxation data analysis was performed using different models described in the theory section. Concerning the overall motion, we have in all the fits used a fixed value of the global correlation time $\tau_M = 5.42$ ns taken from the previous work on the same O-antigen polysaccharide with different labeling (D-[1-^{13}C]glucose). Since the polysaccharide investigated in this work differs from the one used in the earlier work (Lycknert and Widmalm 2004) only by the sites of the carbon-13 labels, it is reasonable to assume that in the dilute solution and at the same temperature global correlation times will be identical (see below).

We started the interpretation of the dynamics of the exocyclic group with the standard Lipari–Szabo model. First, we considered the methyl group in residue **E**, cf. Table 2. The dynamics in general can consist of several types of motions—mainly fast rotation of the methyl group and wobbling of the methyl axis (Skrynnikov et al. 2002). If both these motions are fast, then the standard Lipari–Szabo model, Eq. (6a), should be sufficient. The use of this model requires an assumed dipole–dipole coupling constant or the carbon-proton distance. We choose here to use $r_{CH} = 111.7$ pm, based on the work of Ottiger and Bax (1998). Making use of Eq. (7a), where the generalized order parameter S^2 is adapted to methyl group symmetry, the value in the Table 2 corresponds to $S^2_{ax} = 0.96$. The

Table 1 Summary of the experimental data for the C6 carbons of the CH_2OH and CH_3 groups in the polysaccharide

Field (T)	Residue	T_1 (ms)	T_2 (ms)	NOE
16.4	E	520	141	2.31
	A	255	76	1.74
	D	276	55	1.48
	C	278	45	1.46
21.1	E	558	124	2.25
	A	307	80	1.57
	D	373	54	1.35
	C	374	39	1.39

model yields a fast internal motion correlation time on the order of tens of picoseconds. We note, in passing, that if the τ_M and τ_e values in Table 2 apply, then the longitudinal cross-correlation effects for the methyl group can be neglected (Kay and Torchia 1991). The quality of the fit, measured by the relative error, is not quite satisfactory. Detailed analysis of the results shows that the main part of the disagreement between the experiments and the model comes from the NOEs. This is reminiscent of the observation of Clore et al. (1990), leading to their introduction of the extended Lipari–Szabo model.

For interpretation of the hydroxymethyl dynamics in the residues **A**, **C** and **D**, we begin also with the Lipari–Szabo model, cf. Table 2. Here, we can interpret the generalized order parameter of Lipari–Szabo model in terms of the two-site jump model, Eq. (11). The jump angles obtained using fixed site populations (as discussed above) are also summarized in Table 2. We note that for residue **A** the value of $S^2 = 0.29$ in combination with $P = 0.33$ is in the range where Eq. (11) has no real solution and thus it cannot be interpreted in the terms of two-site jump parameters. Such a low order parameter implies that the motion of the CH_2OH group in residue **A** is very weakly restricted and a two-site jump interpretation is not suitable in this case.

Given the problems with the standard Lipari–Szabo model, we decided to try models allowing for local motion on two different timescales. First, we used the extended Lipari–Szabo model, i.e., Eq. (8a); the results are shown in Table 3. We note that the quality of the fits in Table 3 is generally improved compared to Table 2. For residues **A** and **D**, calculated relative errors of the fit (listed in Tables 2 and 3) are in favor of the extended Lipari–Szabo approach compared to the standard Lipari–Szabo model, while extended Lipari–Szabo fitting does not show significant improvement for residues **E** and **C**. We found that a slow motion of $\tau_s \approx 600$ ps is present for residues **C** and **D**, while $\tau_s \approx 400$ ps for residue **A**. For residue **E**, the slow motion correlation time is over 900 ps. Similarly, the amplitude of slow motion expressed by S^2_s attains the value of $S^2_s \approx 0.5$

Table 2 Fitted parameters from the standard Lipari–Szabo model, based on $r_{CH} = 111.7$ pm

Residue	S^2	τ_e (ps)	P	γ_j [°]	Rel. err. (%)
E	0.107 (0.007)	33.5 (0.9)	N/A	N/A	15.9
A	0.29 (0.02)	275 (21)	0.33 (fixed)	N/S	18.4
D	0.52 (0.06)	413 (408)	0.50 (fixed)	±72	24.1
C	0.56 (0.02)	464 (70)	0.50 (fixed)	±74	9.5

Residues **A**–**E** were fitted separately to the standard Lipari–Szabo model, assuming fast methyl motion (Eqs. 7a, 7b) for residue **E** and using the S^2 of residues **D** and **C** to calculate the jump half-angles γ_j assuming fixed populations P according to Eq. (11) (not possible for residue **A** due to its low S^2). The global correlation time τ_M was fixed to 5.42 ns for each residue. Numbers in the parentheses denote standard deviations based on Monte-Carlo analysis of fitted results. N/A stands for 'not applicable' whereas N/S denotes 'no solution'

for **C** and **D**, while the value for **A** is $S_s^2 \approx 0.3$ and **E** has $S_s^2 = 0.85$. It is worth-while noting that the S_s^2 values for methylene groups in Table 3 are similar to the S^2 in Table 2. Similar dynamics of residues **C** and **D**, while different for **A**, is consistent with the fact that they differ in configuration at the C4 atoms. In addition to the slow local motion, a fast motion at least one order of magnitude faster is present. The amplitude of the fast motion, expressed by $S_f^2 \approx 0.85$ is highly similar in all the hydroxymethyl groups.

The assumption of the fixed global correlation time, taken from the earlier work on a very similar sample, can to a certain extent be validated. For the two residues for which the ordinary Lipari–Szabo approach works well, **C** and **E**, the experimental data sets allow including the third parameter (τ_M) into the fit. The results turned out to be similar for both these residues: the fitted τ_M (not shown) was reduced by about 20 % while the parameters describing the internal motions changed by at most 10 %. For the residues **A** and **D**, which require the extended Lipari–Szabo fit according to the discussion above, we were not able to obtain reasonable fitted τ_M values. However, setting the fixed τ_M to either 5 or 6 ns (instead of 5.42 ns) had also here only a small effect on the internal motion parameters.

Besides the extended Lipari–Szabo model analysis, it is possible to include a certain additional degree of freedom in the random jump model to account for the local motion at different timescales. One can allow for a rapid local motion (vibrations/librations), much faster than the conformational jumps, averaging down the dipole–dipole coupling constant by scaling the r_{CH} distance (Ghalebani et al. 2008). This model was previously applied to γ-cyclodextrin and might also be suitable for investigating the conformational motion of the hydroxymethyl groups in the O-antigen polysaccharide. Based on the results in Table 2, this analysis is only applicable to residues **C** and **D**. Keeping some parameters fixed ($\tau_M = 5.42$ ns, $\theta = 70.5°$, equal site populations), we obtain (not shown) the jump times in the range 500–600 ps (consistent with τ_s from the extended Lipari–Szabo model) and jump angles very close to the values given in Table 2.

The fact that a two-site jump model is appropriate for residues **C** and **D** having the D-*gluco* configuration, but not for the residue **A** possessing D-*galacto* configuration, is consistent with quantum mechanical (QM) potential energy curves of corresponding models for which the barriers to rotation around the ω torsion angle are higher and lower, respectively (Kirschner and Woods 2001). The QM potential energy curves were either of the attractive type where hydrogen bonds (HBs) were allowed to be formed from the hydroxyl proton of the CH_2OH group to the ring oxygen O5 or to the OH group at C4 or of the repulsive type where the corresponding hydrogen bonds were disallowed. In the former cases, for α-D-Glc*p*-OMe and α-D-Gal*p*-OMe, the barriers were closely similar and on the order of ~3.5 kcal mol^{-1} between the *gauche* states and the *trans* conformation, but ~6 kcal mol^{-1} between the *gauche* states. In the latter cases (HBs not allowed), the barriers for the *gluco*-configuration were high, ~7–8 kcal mol^{-1}, whereas the barrier for the *galacto*-configuration between the *gauche-trans* and the *trans-gauche* states was small, ~2 kcal mol^{-1}, a difference in line with the ^{13}C NMR relaxation data obtained for the different sugars carrying a hydroxymethyl group (Fig. 3) in this study, especially the low S^2 value in residue **A**.

It is interesting to compare the results of the extended Lipari–Szabo model analysis in Table 3 with similar data from Lycknert and Widmalm (2004) for the same polysaccharide with a different ^{13}C-labeling. The comparison for the residue **C** is not straight forward, because the earlier work included an exchange contribution, absent here. However, the exchange rate is very low (2.7 s^{-1}) and we neglect it for the purposes of qualitative comparison here. In the analysis of the hydroxymethyl groups of the residues **A**, **C** and **D**, the S^2 (and S_s^2) values obtained here are clearly lower than the corresponding numbers from the Lipari–Szabo (0.63 for **A**, 0.64 for **D**, and 0.62 for **C** residue) in the earlier work based on the [1-^{13}C]-labeling scheme. Concerning the correlation times, the slow local correlation time for the residue **A** here (381 ps) is closely similar to the previous result (387 ps), while τ_s for residues **D** and **C** are somewhat longer in the present study (~600 ps compared to ~400 ps in the previous study). For the methyl group in residue **E**, our τ_s is longer (946 ps) than the local correlation time for this residue in the previous study (517 ps). Consistently with the earlier work, the τ_s for residue **E** is the longest in the whole repeating unit.

We interpret tentatively the decreased order parameter as indicating the presence of an additional motion

Table 3 Fitted parameters from the extended Lipari–Szabo model, based on $r_{CH} = 111.7$ pm

Residue	S^2	S_f^2	$S_s^2 = S^2/S_f^2$	τ_s [ps]	τ_f [ps]	Rel. Err. [%]
E	0.092 (0.01)	0.11	0.85	946 (173)	31 (1)	17.2
A	0.22 (0.02)	0.84 (0.07)	0.26	381 (135)	15 (26)	1.7
D	0.37 (0.05)	0.84 (0.04)	0.44	555 (496)	0 (25)	3.1
C	0.50 (0.05)	0.90 (0.05)	0.56	645 (342)	47 (40)	8.2

All the residues were fitted separately; the global correlation time τ_M was fixed to 5.42 ns for each residue. For residues **A** and **D** the fast correlation time converges to zero. Numbers in the parentheses denote standard deviations based on Monte-Carlo analysis of fitted results. For residue **E**, S_f^2 attains the maximum value consistent with fast reorientation of the methyl group

influencing the relaxation of the hydroxymethyl groups. Besides the breathing motion of a loosely folded polymer, already observed for the sugar rings with the [1-^{13}C]-labeling, one or two other types of motions are present. For residues **C** and **D**, one motion occurs most probably on a timescale similar to the breathing motion of the polysaccharide chain, the other one is one order of magnitude faster. Based on the previous extended Lipari–Szabo model and two-site jump analysis we can associate the slow motion to the conformational jump and the fast motion to the highly restricted motion at the potential energy minima. The situation is different for the residue **A**, where the slow motion seems to reflect the weakly restricted rotation of the CH_2OH group around the C5–C6 axis. For the correlation times we conclude that, if the comparison is made at the level of the Lipari–Szabo model (Table 2), then the local correlation times in the present work are shortened with respect to the previous study, which supports the idea with the two types of motions occurring on a similar time scale.

The O-antigen polysaccharide from *E. coli* O91 is built of repeating units having five sugar residues with highly similar generalized order parameters $S^2 \approx 0.63$, based on the [1-^{13}C]-labeling in the previous study (Lycknert and Widmalm 2004). However, along the polymer chain, in which each sugar is linked to a secondary carbon atom resulting in quite similar linkages, a trend is observed with varying effective correlation times (τ_e) as a function of sugar residue where the sequential difference in τ_e is small between subsequent residues. The additional dynamics of exocyclic groups observed herein based on the [6-^{13}C]-labeling adds conformational dynamics to this polymer. Two of the sugar residues are also substituted by additional functional groups, viz., a glycine residue linked as an amide to C6 of residue **B** and an (*R*)-3-hydroxybutyramido group linked as an amide to the N3 atom of residue **E**. One may thus envision the polysaccharide as a polymer made of beads on a string with flexible attachments to the beads. The biological implication of this as part of a lipopolysaccharide in the outer membrane of *E. coli* bacteria remains to be elucidated.

In conclusion, comparing the performance of the different models for hydroxymethyl group dynamics, the extended Lipari–Szabo model accounting for two different timescales of the local motion interpret the relaxation data quite well. Magnitude of the half-angle from the two-site jump model is consistent with a slightly larger torsion angle of $\approx 65°$ used when conformational equilibria are analyzed for the ω torsion angle (Stenutz et al. 2002), even though the effective C–H distances become somewhat longer. Throughout all the models, noticeably similar dynamics of the residues **C** and **D** is obtained, while residue **A** behaves differently. This is consistent with the fact that the residues differ in configuration at the C4 atoms.

Acknowledgments This work was supported by the Swedish Research Council (Grant Number 613-2011-3311 and 621-2010-4890). The generous Grant from the Knut and Alice Wallenberg Foundation, allowing for the purchase of the 700 MHz NMR spectrometer for the Arrhenius Laboratory, is gratefully acknowledged. Financial support in the form of Access to the Bio-NMR Research Infrastructure co-funded under the 7th Framework Programme of the EC (FP7/2007-2013) Grant agreement 261863 for conducting the research is gratefully acknowledged. The work was also supported by the Grant SVV-2012-265305 from the Czech ministry of education.

References

Brondeau J, Canet D (1977) Longitudinal magnetic relaxation of ^{13}C (or ^{15}N) interacting with a strongly irradiated proton system. J Chem Phys 67:3650–3654

Carriere CJ, Amis EJ, Schrag JL, Ferry JD (1993) Dilute-solution dynamic viscoelastic properties of xanthan polysaccharide. J Rheol 37:469–478

Chatfield DC, Szabo A, Brooks BR (1998) Molecular dynamics of staphylococcal nuclease: comparison of simulation with ^{15}N and ^{13}C relaxation data. J Am Chem Soc 120:5301–5311

Chytil M, Strand S, Christensen BE, Pekar M (2010) Calorimetric and light scattering study of interactions and macromolecular properties of native and hydrophobically modified hyaluronan. Carbohydr Polym 81:855–863

Clore GM, Szabo A, Bax A, Kay LE, Driscoll PC, Gronenborn AM (1990) Deviations from the simple two-parameter model-free approach to the interpretation of nitrogen-15 nuclear magnetic relaxation of proteins. J Am Chem Soc 112:4989–4991

Ferrage F, Reichel A, Battacharya S, Cowburn D, Ghose R (2010) On the measurement of ^{15}N-{^{1}H} nuclear Overhauser effects. 2. Effects of the saturation scheme and water signal suppression. J Magn Reson 207:294–303

Ghalebani L, Kotsyubynskyy D, Kowalewski J (2008) NMR relaxation interference effects and internal dynamics in γ-cyclodextrin. J Magn Reson 195:1–8

Gitti R, Long G, Bush CA (1994) Measurement of long-range2 ^{13}C-^{1}H coupling constants of 95% uniformly ^{13}C-labeled polysaccharide from *Streptococcus mitis* J22. Biopolymers 34: 1327–1338

Henderson TJ, Venable RM, Egan W (2003) Conformational flexibility of the group B meningococcal polysaccharide in solution. J Am Chem Soc 125:2930–2939

Hills BP, Cano C, Belton PS (1991) Proton NMR relaxation studies of aqueous polysaccharide systems. Macromolecules 24:2944–2950

Hricovini M, Guerrini M, Torri G, Casu B (1997) Motional properties of *E. Coli* polysaccharide K5 in aqueous solution analyzed by NMR relaxation measurements. Carbohydr Res 300:69–76

Jasnin M, Van Eijck L, Koza MM, Peters J, Laguri C, Lortat-Jacob H, Zaccai G (2010) Dynamics of heparan sulfate explored by neutron scattering. Phys Chem Chem Phys 12:3360–3362

Kay LE, Bull TE (1992) Heteronuclear transverse relaxation in AMX, AX_2, and AX_3 spin systems. J Magn Reson 99:615–622

Kay LE, Torchia DA (1991) The effects of dipolar cross correlation on ^{13}C methyl-carbon T_1, T_2, and NOE measurements in macromolecules. J Magn Reson 95:536–547

Kay LE, Nicholson LK, Delaglio F, Bax A, Torchia DA (1992) Pulse sequences for removal of the effects of cross correlation between dipolar and chemical-shift anisotropy relaxation mechanism on the measurement of heteronuclear T_1 and T_2 values in proteins. J Magn Reson 97:359–375

Kirschner KN, Woods RJ (2001) Solvent interactions determine carbohydrate conformation. Proc Natl Acad Sci USA 98: 10541–10545

Kjellberg A, Weintraub A, Widmalm G (1999) Structural determination and biosynthetic studies of the O-antigenic polysaccharide from the enterohemorrhagic *Escherichia coli* O91 using ^{13}C-enrichment and NMR spectroscopy. Biochemistry 38:12205–12211

Knirel YA, Volvano MA (eds) (2011) Bacterial lipopolysaccharides. Structure, chemical synthesis, biogenesis and interaction with host cells. Springer, Wien

Kövér KE, Batta G, Kowalewski J, Ghalebani L, Kruk D (2004) Internal dynamics of hydroxymethyl rotation from CH_2 cross-correlated dipolar relaxation in methyl-β-D-glucopyranoside. J Magn Reson 167:273–281

Kowalewski J, Mäler L (2006) Nuclear spin relaxation in liquids. Taylor and Francis, New York

Lawrence JG (1999) Gene transfer, speciation, and the evolution of bacterial genomes. Curr Opin Microbiol 2:519–523

Lipari G, Szabo A (1982) Model-free approach to the interpretation of nuclear magnetic resonance relaxation in macromolecules 1. Theory and range of validity. J Am Chem Soc 104:4546–4559

London RE (1978) On the interpretation of ^{13}C spin-lattice relaxation resulting from ring puckering in proline. J Am Chem Soc 100:2678–2685

Lycknert K, Widmalm G (2004) Dynamics of the *Escherichia coli* O91 O-antigen polysaccharide in solution as studied by carbon-13 NMR relaxation. Biomacromolecules 5:1015–1020

Millet O, Muhandiram DR, Skrynnikov NR, Kay LE (2002) Deuterium spin probes of side-chain dynamics in proteins. 1. Measurement of five relaxation rates per deuteron in ^{13}C-labeled and fractionally ^{2}H-enriched proteins in solution. J Am Chem Soc 124:6439–6448

Norris SE, Landström J, Weintraub A, Bull TE, Widmalm G, Freedberg DI (2012) Transient hydrogen bonding in uniformly ^{13}C,^{15}N-labeled carbohydrates in water. Biopolymers 97:145–154

Nyberg NT, Duus JØ, Sørensen OW (2005) Heteronuclear two-bond correlation: suppressing heteronuclear three-bond or higher NMR correlations while enhancing two-bond correlations even for vanishing $^{2}J_{CH}$. J Am Chem Soc 127:6154–6155

Olsson U, Säwén E, Stenutz R, Widmalm G (2009) Conformational flexibility and dynamics of two (1 → 6)-linked disaccharides related to an oligosaccharide epitope expressed on malignant tumour cells. Chem Eur J 15:8886–8894

Ottiger M, Bax A (1998) Determination of relative N-HN, N–C′, Cα–C′, and Cα–Hα effective bond lengths in a protein by NMR in a dilute liquid crystalline phase. J Am Chem Soc 120:12334–12341

Palmer AG, Skelton NJ, Chazin WJ, Wright PE, Rance M (1992) Suppression of the effects of cross-correlation between dipolar and anisotropic chemical shift relaxation mechanisms in the measurement of spin–spin relaxation rates. Mol Phys 75:699–711

Rédini F (ed) (2012) Proteoglycans. Meth Mol Biol vol 836. Humana Press, New York

Skrynnikov NR, Millet O, Kay LE (2002) Deuterium spin probes of side-chain dynamics in proteins. 2. Spectral density mapping and identification of nanosecond time-scale side-chain motions. J Am Chem Soc 124:6449–6460

Stenutz R, Carmichael I, Widmalm G, Serianni AS (2002) Hydroxymethyl group conformation in saccharides: structural dependencies of $^{2}J_{HH}$, $^{3}J_{HH}$, and $^{1}J_{CH}$ spin–spin coupling constants. J Org Chem 67:949–958

Stenutz R, Weintraub A, Widmalm G (2006) The structures of *Escherichia coli* O-polysaccharide antigens. FEMS Microbiol Rev 30:382–403

Tang D, Li A, Attar P, Dowell EH (2004) Reduced order dynamic model for polysaccharides molecule attached to an atomic force microscope. J Comput Phys 201:723–752

Vlachou S, Politou A, Dais P, Mazeau K, Taravel FR (2001) Structure and dynamics of the branched polysaccharide scleroglucan in dilute solutions studied by 1D and 2D NMR spectroscopy. Carbohydr Polym 46:349–363

Werbelow LG, Grant DM (1977) Intramolecular dipolar relaxation in multispin systems. Adv Magn Reson 9:189–299

Widmalm G, Pastor RW, Bull TE (1991) Molecular dynamics simulation of methyl group relaxation in water. J Chem Phys 94:4097–4098

Yother J (2011) Capsules of *Streptococcus pneumoniae* and other bacteria: paradigms for polysaccharide biosynthesis and regulation. Annu Rev Microbiol 65:563–581

Zerbetto M, Polimeno A, Kotsyubynskyy D, Ghalebani L, Kowalewski J, Meirovitch E, Olsson U, Widmalm G (2009) An integrated approach to NMR spin relaxation in flexible biomolecules: application to β-D-glucopyranosyl-(1 → 6)-α-D-mannopyranosyl-OMe. J Chem Phys 131:234501

Zhu LY, Kemple MD, Landy SB, Buckley P (1995) Effect of dipolar cross correlation on model-free motional parameters obtained from ^{13}C relaxation in AX_2 systems. J Magn Reson Ser B 109:19–30